Short range correlations in the weak decay of Λ hypernuclei

A. Parreño and A. Ramos
Departament d'Estructura i Constituents de la Matèria, Universitat de Barcelona, Diagonal 647, 08028 Barcelona, Spain

E. Oset
Departamento de Física Teórica and IFIC, Centro Mixto Universidad de Valencia-CSIC, 46100 Burjassot, Valencia, Spain
(Received 12 September 1994)

The differences found in the relativistic and nonrelativistic methods used in the literature to account for short range nuclear correlations in the decay of Λ hypernuclei are analyzed. By means of a schematic microscopic model for the origin of correlations, the appropriate method to include them in nuclear processes is derived and is found to be the same one used in the nonrelativistic approach. The differences do not stem from relativistic effects but from the improper implementation of the correlations in the relativistic approach, which leads to several pathologies as shown in the paper. General formulas are given to evaluate the nonmesonic decay width of finite hypernuclei and results are obtained for ${}^{5}_{\Lambda}$He and ${}^{12}_{\Lambda}$C.

PACS number(s): 21.80.+a

I. INTRODUCTION

When stable against particle emission, Λ-hypernuclei decay through weak interaction processes which do not involve leptons. Studying the hypernuclear decay modes may help to shed some light on the strong interaction corrections to the basic weak interaction. The mesonic mode ($\Lambda \to \pi N$) is highly supressed in the nuclear medium due to Pauli blocking acting on the emitted nucleon, which has a momentum of about 100 MeV/c. In the nonmesonic $\Lambda N \to NN$ process, where the pion can be viewed as being absorbed by another nucleon, there is no Pauli blocking since the two nucleons emerge with a large momentum of about 400 MeV/c. Therefore, the decay of all but the lightest Λ hypernuclei proceeds mainly through the nonmesonic mode $\Lambda N \to NN$, which, since the pioneering work of Adams [1], has received much theoretical attention [2–7]. Although the two-body-induced nonmesonic mode $\Lambda NN \to NNN$ was found to be relatively important [8], a recent calculation, which uses a more realistic input for the pion optical potential and takes into consideration the available phase space for two-particle–two-hole excitation, finds that this decay mode only amounts to about 15% of the total decay rate [9].

The large momentum of the emitted nucleons in the $\Lambda N \to NN$ channel makes this decay mode quite insensitive to nuclear structure details and, therefore, it can provide useful information to learn about the weak interaction at the hadronic level. On the other hand, the large momentum carried by the exchanged meson indicates that the distances probed by this process are relatively small and the effect of strong short range correlations between the interacting ΛN pair can be quite important. This was indeed found to be the case for the nonrelativistic calculations in nuclear matter [2–4], where the nonmesonic rate was reduced by a factor of up to 2. Surprisingly, the relativistic calculation of Ref. [7] in ${}^{12}_{\Lambda}$C found twice as much reduction with a similar correlation function. However, it is difficult to reconcile this discrepancy within the new ingredients of Ref. [7], namely, the use of a relativistic formalism based on Dirac phenomenology, and the consideration of a finite system rather than nuclear matter. On the one hand, Ref. [7] showed that both relativistic and nonrelativistic calculations give very similar rates in the absence of correlations while, on the other hand, one expects the size of the system to be irrelevant in understanding short range phenomena which occur at distances smaller than one fermi.

It is the purpose of the present work to understand the origin of such discrepancies. In Sec. II, we show that the explanation can be traced to the way the correlations are implemented. The relativistic calculations use pseudoscalar πNN couplings at the vertices and their matrix elements are evaluated with spinors carrying the external quantum numbers. The nonrelativistic procedure, which assumes a pseudovector coupling at the strong πNN vertex with the derivative acting on the pion field, is shown to be equivalent to what is obtained from a microscopic model for the short range correlations. This microscopic model, developed in Sec. II, shows that the essential point is that the matrix elements of the πNN and $\pi N\Lambda$ couplings must contain the intermediate momentum states excited by the exchange of heavy mesons originating the correlations. In Sec. III the elementary $\Lambda N \to NN$ correlated transition amplitude is obtained for the two prescriptions, and the expression for the decay rate of finite nuclei in terms of a correlated potential in r space is given. This r-space potential is derived in Sec. IV. A numerical comparative study of both prescriptions in the weak decay of ${}^{5}_{\Lambda}$He is done in Sec. V. Final results for the nonmesonic decay rate of ${}^{5}_{\Lambda}$He and ${}^{12}_{\Lambda}$C with the proper prescription for short range correlations and incorporating form factors at the vertices are also discussed in Sec. V. Some concluding remarks are given in Sec. VI.

II. CORRELATED FEYNMAN AMPLITUDE

The starting point for our derivation is the Feynman diagram of Fig. 1 which is given by the expression

$$\mathcal{M}_\pi = \int d^4x d^4y \overline{\psi}_{p_3}(x)\Gamma_1\psi_{p_1}(x)\Delta_\pi(x-y) \times \overline{\psi}_{p_4}(y)\Gamma_2\psi_{p_2}(y) \ , \quad (1)$$

where

$$\psi_{p_i}(x) = e^{-ip_i x_i}u(p_i) \quad (2)$$

is the free baryon field of positive energy, Γ_i the Dirac operator characteristic of the baryon-baryon-pion vertex, and

$$\Delta_\pi(x-y) = \int \frac{d^4q}{(2\pi)^4}\frac{e^{iq(x-y)}}{(q^0)^2-\mathbf{q}^2-\mu^2} \quad (3)$$

the pion propagator, where μ is the pion mass.

Assume now that the two-body process illustrated in Fig. 1 takes place in the nuclear medium. One may consider a phenomenological way of taking the short range correlations (SRC's) between the initial particles into account by including in Eq. (1) an appropriate pair correlation function $f(x-y)$, which simulates the strong repulsion at short relative distances generated by the exchange of heavy mesons between the interacting pair of particles.

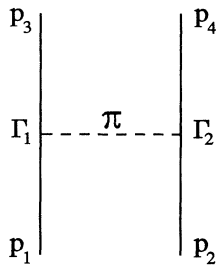

FIG. 1. Illustration of the Feynman diagram for the two-body transition amplitude $B_1B_2 \to B_3B_4$.

Using Eqs. (2) and (3), performing a change to center-of-mass and relative variables

$$\mathbf{x}+\mathbf{y} = 2\mathbf{R}, \quad \mathbf{x}-\mathbf{y} = \mathbf{r} \ , \quad (4)$$

where the masses of the particles have been assumed to be identical for simplicity, and integrating over $\mathbf{R}$, time, and energy variables, one easily derives (except for an energy conserving delta function)

$$\tilde{\mathcal{M}}(p_1,p_3) = \int d^3r e^{i(\mathbf{p}_1-\mathbf{p}_3)\mathbf{r}}f(r)\int \frac{d^3q}{(2\pi)^3}\overline{u}(p_3)\Gamma_1 u(p_1)\frac{e^{-i\mathbf{q}\cdot\mathbf{r}}}{(q^0)^2-\mathbf{q}^2-\mu^2}\overline{u}(p_4)\Gamma_2 u(p_2), \quad (5)$$

with $q^0 = p_1^0 - p_3^0 = p_4^0 - p_2^0$ and $\mathbf{p}_1 - \mathbf{p}_3 = \mathbf{p}_4 - \mathbf{p}_2$. In Eq. (5), the correlation function has been assumed to be static and depending only on the modulus of the relative distance, $r = |\mathbf{x}-\mathbf{y}|$, which is justified by the short range nature of the strong interaction inducing the correlations.

The vertex $\overline{u}(p')\Gamma u(p)$ comes from the matrix element between fields,

$$\overline{\psi}(x)\Gamma\psi(x), \quad (6)$$

when only the parts of the field corresponding to the positive energy states are considered. For the case of the πNN strong coupling and on-shell positive energy components, two types of vertices, pseudoscalar ($\Gamma_{PS} = ig_{\pi NN}\gamma_5$) and pseudovector ($\Gamma_{PV} = -\frac{g_{\pi NN}}{2M}\gamma_5\gamma^\mu\partial_\mu$), are known to give the same matrix elements, i.e.,

$$\overline{\psi}^{(-)}(x)i\gamma_5\psi^{(+)}(x) \equiv -\partial_\mu\left[\overline{\psi}^{(-)}(x)\frac{1}{2M}\gamma_5\gamma^\mu\psi^{(+)}(x)\right] \ , \quad (7)$$

with M the nucleon mass and $\psi^{(+)}$, $\overline{\psi}^{(-)}$ the parts of the fields attached to the positive energy components. Equivalently, we can express Eq. (7) as

$$\overline{u}(p')i\gamma_5 u(p) = \frac{i}{2M}(p-p')_\mu\overline{u}(p')\gamma_5\gamma^\mu u(p) \ . \quad (8)$$

Using the fact that the addition of a total derivative of a Lagrangian leaves the equations of motion invariant, the identity in Eq. (7) can be expressed as

$$\overline{\psi}^{(-)}(x)i\gamma_5\psi^{(+)}(x)\Phi(x) \equiv \overline{\psi}^{(-)}(x)\frac{1}{2M}\gamma_5\gamma^\mu\psi^{(+)}(x)\partial_\mu\Phi(x) \ , \quad (9)$$

with $\Phi(x)$ the pion field, which is a more common way of establishing the equivalence between pseudoscalar and pseudovector couplings in the case of plane waves.

By using the equivalence of the two couplings in the form of Eq. (7) or (8) and going to the usual nonrelativistic limit, we obtain in both cases the vertex

$$i\frac{g_{\pi NN}}{2M}\boldsymbol{\sigma}(\mathbf{p}-\mathbf{p}'). \quad (10)$$

Therefore, assuming $q^0 = 0$, the nonrelativistic reduction of Eq. (5) gives for both cases

$$\tilde{M}(\mathbf{k}) = -\frac{g^2_{\pi NN}}{4M^2}\boldsymbol{\sigma}_1\mathbf{k}\,\boldsymbol{\sigma}_2\mathbf{k}\int d^3r e^{i\mathbf{k}\cdot\mathbf{r}} f(r)\int\frac{d^3q}{(2\pi)^3}\frac{e^{-i\mathbf{q}\cdot\mathbf{r}}}{\mathbf{q}^2+\mu^2}$$

$$= -\frac{g^2_{\pi NN}}{4M^2}\boldsymbol{\sigma}_1\mathbf{k}\,\boldsymbol{\sigma}_2\mathbf{k}\int d^3r e^{i\mathbf{k}\cdot\mathbf{r}} f(r)\frac{e^{-\mu r}}{4\pi r}\ , \qquad (11)$$

where $\mathbf{k} = \mathbf{p}_1 - \mathbf{p}_3$.

Now let us take the pseudovector coupling in the form of Eq. (9). The derivative ∂_μ acts now on the pion field in the pion propagator. Since, according to Eq. (3), the pion momentum is $\mathbf{q}$, a nonrelativistic reduction of Eq. (5) now gives

$$\tilde{M}(\mathbf{k}) = -\frac{g^2_{\pi NN}}{4M^2}\int d^3r e^{i\mathbf{k}\cdot\mathbf{r}} f(r)$$
$$\times\int\frac{d^3q}{(2\pi)^3}\frac{e^{-i\mathbf{q}\cdot\mathbf{r}}}{\mathbf{q}^2+\mu^2}\boldsymbol{\sigma}_1\mathbf{q}\,\boldsymbol{\sigma}_2\mathbf{q}\ . \qquad (12)$$

The main difference between Eqs. (11) and (12) lies in the fact that the quantities $\boldsymbol{\sigma}\mathbf{q}$ do not factorize out of the integral over $\mathbf{q}$ in Eq. (12) and the Yukawa shape of Eq. (11) is not recovered. Instead, the integral over $\mathbf{q}$ gives the typical one-pion-exchange (OPE) potential consisting of a central and a tensor piece:

$$V_{\rm OPE}(\mathbf{r}) = V_C(r)\boldsymbol{\sigma}_1\boldsymbol{\sigma}_2 + V_T(r)S_{12}(\hat{\mathbf{r}}), \qquad (13)$$

with $S_{12}(\hat{\mathbf{r}}) = 3\boldsymbol{\sigma}_1\hat{\mathbf{r}}\boldsymbol{\sigma}_2\hat{\mathbf{r}} - \boldsymbol{\sigma}_1\boldsymbol{\sigma}_2$ and

$$V_C(r) = \frac{g^2_{\pi NN}}{4M^2}\frac{1}{3}\left(\mu^2\frac{e^{-\mu r}}{4\pi r} - \delta(\mathbf{r})\right),$$

$$V_T(r) = \frac{g^2_{\pi NN}}{4M^2}\frac{1}{3}\mu^2\frac{e^{-\mu r}}{4\pi r}\left(1+\frac{3}{\mu r}+\frac{3}{(\mu r)^2}\right)\ .$$

By inspecting the form of Eq. (12) for $\tilde{M}(\mathbf{k})$, one realizes that it is already the Fourier transform of the $\mathbf{r}$-dependent quantity

$$\tilde{V}(\mathbf{r}) = V_{\rm OPE}(\mathbf{r})f(r)\ , \qquad (14)$$

which is directly identified with the correlated potential in r space. Since correlations are now present in the potential, any transition matrix element from an initial to a final state must be evaluated with an uncorrelated wave function

$$\langle\psi_{\rm fin}|\,\tilde{V}\,|\phi_{\rm ini}\rangle \propto \int d^3r\psi^*_{\rm fin}(\mathbf{r})V_{\rm OPE}(\mathbf{r})f(r)\phi_{\rm ini}(\mathbf{r}). \qquad (15)$$

It is clear that Eq. (15) is equivalent to the transition amplitude for the bare potential [Eq. (13)] starting from an initial correlated wave function, $\langle\psi_{\rm fin}|\,V_{\rm OPE}\,|\psi_{\rm ini}\rangle$, provided one identifies

$$\psi_{\rm ini}(\mathbf{r}) = f(r)\phi_{\rm ini}(\mathbf{r})\ , \qquad (16)$$

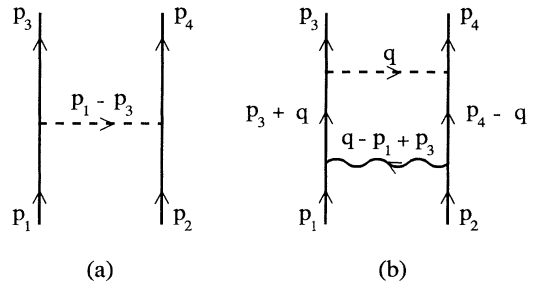

FIG. 2. Schematic model to include correlations in the OPE potential. Bare one-pion-exchange diagram (a) and one-pion exchange with simultaneous exchange of a heavy meson responsible for the short range repulsion (b).

which, in a first approximation, is the usual procedure in the study of strong transition amplitudes.

It is curious to see that the use of two equivalent Lagrangians gives rise to different results once the effect of short range correlations is taken into account and this calls for an answer. Meanwhile, we can already reach some clarifying conclusion: The different effects of correlations found in the relativistic calculation of Ref. [7] as compared to the nonrelativistic ones [2–4] have nothing to do with relativistic effects. They are due to the different way in which the correlations are handled. In Ref. [7] the effect of correlations appeared as in Eq. (11), factorizing a Yukawa function, while in Refs. [2–4] it appeared as in Eq. (12), factorizing the OPE potential with a scalar and a tensor part.

Next we show that, even if intuitive, the way of implementing the short range correlations which led to Eq. (11) is incorrect and the proper method is the one that leads to Eq. (12). To reach this conclusion we must go back to the microscopic origin of short range correlations. In the meson exchange model, they arise because of the simultaneous exchange of heavy mesons together with one-pion exchange. The picture, simplified to include only one extra heavy meson (assume it a vector meson like the ω), is shown in Fig. 2. The intermediate nucleon states in Fig. 2(b) are assumed to be positive energy states and the potentials due to the exchange of mesons are taken to be static as in the usual studies of nuclear correlations. The uncorrelated OPE of Fig. 2(a) leads to the amplitude

$$\tilde{M} = g^2_{\pi NN}\bar{u}(p_3)\gamma_5 u(p_1)\frac{1}{\mathbf{k}^2+\mu^2}\bar{u}(p_4)\gamma_5 u(p_2) \qquad (17)$$

or, in the nonrelativistic limit,

$$\tilde{M} = -\frac{g^2_{\pi NN}}{4M^2}\frac{\boldsymbol{\sigma}_1\mathbf{k}\,\boldsymbol{\sigma}_2\mathbf{k}}{\mathbf{k}^2+\mu^2}\ , \qquad (18)$$

with $\mathbf{k} = \mathbf{p}_1 - \mathbf{p}_3$. On the other hand, the potential equivalent to Fig. 2(b) will be given by

$$-i\tilde{M} = \int\frac{d^4q}{(2\pi)^4}i^2 g^2_{\omega NN}\frac{-i}{-(\mathbf{q}-\mathbf{p}_1+\mathbf{p}_3)^2-m^2_\omega}\frac{i}{-\mathbf{q}^2-\mu^2}$$
$$\times\frac{i}{p^0_4-q^0-E(\mathbf{p}_4-\mathbf{q})+i\epsilon}\frac{i}{p^0_3+q^0-E(\mathbf{p}_3+\mathbf{q})+i\epsilon}Qg^2_{\pi NN}\bar{u}(p_3)\gamma_5 u(p_3+q)\bar{u}(p_4)\gamma_5 u(p_4-q)\ , \qquad (19)$$

where we have taken the usual nonrelativistic approach to ω exchange which selects the $-g^{00}$ component of the propagator with ωNN vertices of the γ^μ type. In Eq. (19), $E(\mathbf{p})$ is the nucleon energy and Q the Pauli blocking operator acting on the intermediate states. By carrying out the q^0 integration we obtain

$$\tilde{M} = \int \frac{d^3q}{(2\pi)^3} \frac{g^2_{\omega NN}}{(\mathbf{q}-\mathbf{p}_1+\mathbf{p}_3)^2+m^2_\omega} \frac{1}{\mathbf{q}^2+\mu^2} \frac{Q}{p_3^0+p_4^0-E(\mathbf{p}_3+\mathbf{q})-E(\mathbf{p}_4-\mathbf{q})+i\epsilon} \times g^2_{\pi NN}\overline{u}(p_3)\gamma_5 u(p_3+q)\overline{u}(p_4)\gamma_5 u(p_4-q) \ . \tag{20}$$

In order to connect with the former expressions we take the usual nonrelativistic limit and obtain

$$\tilde{M} = -\frac{g^2_{\pi NN}}{4M^2} \int \frac{d^3q}{(2\pi)^3} \frac{g^2_{\omega NN}}{(\mathbf{q}-\mathbf{p}_1+\mathbf{p}_3)^2+m^2_\omega} \frac{\boldsymbol{\sigma}_1\mathbf{q}\,\boldsymbol{\sigma}_2\mathbf{q}}{\mathbf{q}^2+\mu^2} \frac{Q}{p_3^0+p_4^0-E(\mathbf{p}_3+\mathbf{q})-E(\mathbf{p}_4-\mathbf{q})+i\epsilon} \ . \tag{21}$$

Note that the operator $\boldsymbol{\sigma}_1\mathbf{q}\,\boldsymbol{\sigma}_2\mathbf{q}$ appears inside the integral over $\mathbf{q}$ like in Eq. (12) and does not factorize out as $\boldsymbol{\sigma}_1\mathbf{k}\,\boldsymbol{\sigma}_2\mathbf{k}$ like in Eq. (11). Since the correlated potential corresponds to summing the contributions from Figs. 2(a) and 2(b), by writing the correlation function $f(r)$ as

$$f(r) = 1 - g(r) \ , \tag{22}$$

the sum of Eqs. (21) and (18) can be identified with Eq. (12) by means of the equivalence

$$\int d^3r e^{i(\mathbf{k}-\mathbf{q})\cdot\mathbf{r}} g(r) \simeq -\frac{g^2_{\omega NN}}{(\mathbf{q}-\mathbf{k})^2+m^2_\omega} \frac{Q}{p_3^0+p_4^0-E(\mathbf{p}_3+\mathbf{q})-E(\mathbf{p}_4-\mathbf{q})+i\epsilon} \ . \tag{23}$$

The former relation replaces the effect of correlations by a local and energy-independent function, which is shown to be a good approximation in the case of very short range strong repulsion [10]. The equivalence (23) can also be illustrated in the following way: Assuming the initial interacting nucleons at rest ($\mathbf{p}_1 = \mathbf{p}_2 = \mathbf{0}$), the outgoing momenta must be very large due to the effect of the strongly repulsive core at short distances. Therefore, one can approximate $\mathbf{k} = \mathbf{p}_1 - \mathbf{p}_3 = \mathbf{p}_4 - \mathbf{p}_2$ by $\mathbf{k} \simeq -\mathbf{p}_3 \simeq \mathbf{p}_4$ and the second term in Eq. (23) turns out to be a function of $|\ \mathbf{k}-\mathbf{q}\ |$ as in the first term.

By means of Eq. (23) one can easily compare Eq. (20) with Eq. (5) taking $\Gamma = i\gamma_5$. The essential difference is that instead of $\overline{u}(p_3)\Gamma u(p_1)$ and $\overline{u}(p_4)\Gamma u(p_2)$, as in Eq. (5), one has now $\overline{u}(p_3)\Gamma u(p_3+q)$ and $\overline{u}(p_4)\Gamma u(p_4-q)$ involving intermediate spinors. In this way the matrix elements become q dependent rather than q independent as in Eq. (11). The diagram of Fig. 2(b), which gives a microscopic interpretation for the origin of correlations, clearly shows that the bare interaction connects the final states with intermediate spinors which are q dependent.

The important point we have learned from this model is that, in the construction of the correlated amplitude, the vertices of the bare OPE potential must enter the $\mathbf{q}$ integration as a function of $\mathbf{q}$ instead of factorizing out as functions of the external variables as happened in the derivation that led to Eq. (11). As we will show in Sec. III, the nonmesonic $\Lambda N \to NN$ transition amplitude has a parity conserving piece involving the use of pseudoscalar (or pseudovector) couplings at the vertices and thus the arguments so far developed apply also to this hypernuclear decay mode. As pointed out before, these arguments explain the different effect of correlations on the weak decay of hypernuclei found by the nonrelativistic [2–4] and the relativistic [7] calculations. In Ref. [7], the matrix elements of the couplings are evaluated between spinors carrying the external momenta, while the microscopic model requires them to be evaluated between an external spinor and a spinor carrying the momentum of the intermediate state which is excited by the exchange of the heavy meson originating the short range correlations. From our microscopic model we conclude that the form of the correlated potential as in Eq. (12) is the appropriate one, which is obtained if one starts from the OPE potential in coordinate space and multiplies it by a correlation function as done in Refs. [2–4]. In fact, we have shown that this appropriate correlated potential can equivalently be obtained by following the steps of Ref. [7] sketched at the beginning of this section, which led to Eq. (5), and using a pseudovector coupling in the form of Eq. (8), which leads to Eq. (12). Instead, if a pseudoscalar coupling or a pseudovector coupling in the form of Eq. (7) is used in Eq. (5), one obtains, as in Ref. [7], the correlated potential of Eq. (11) which is not what a microscopic interpretation of the SRC's predicts.

III. NONMESONIC WEAK $\Lambda N \to NN$ TRANSITION

The transition $\Lambda N \to NN$ can be represented by the diagram of Fig. 1, where now p_1 denotes the four-momentum of the Λ and Γ_1, Γ_2 are the weak and strong vertices, respectively. The weak vertex Hamiltonian for the one-pion-exchange mechanism is parametrized as

$$\mathcal{H}_{\Lambda N\pi} = iG_F\mu^2\overline{\psi}_N(A - B\gamma_5)\boldsymbol{\tau}\boldsymbol{\phi}_\pi\psi_\Lambda \ , \tag{24}$$

where $G_F\mu^2 = 2.21 \times 10^{-7}$ is the weak coupling constant. The empirical constants $A = 1.05$ and $B = 7.15$,

which are adjusted to the observables of the free Λ decay, determine the strength of the parity violating (PV) and parity conserving (PC) amplitudes, respectively. The nucleon and pion fields are given by ψ_N and $\boldsymbol{\phi}_\pi$, respectively, while the lambda field ψ_Λ is taken as the spurion isospin state $|t\, m_t\rangle = |1/2\ -1/2\rangle$ to enforce the empirical $\Delta I = 1/2$ rule observed in the decay of a free Λ.

The correlated PC amplitude, involving pseudoscalar (or pseudovector) couplings for both pion vertices in the diagrams of Fig. 2, will be given by Eq. (12) with the replacement

$$\frac{g^2_{\pi NN}}{4M^2} \longrightarrow -\frac{G_F\mu^2 B}{2\overline{M}}\frac{g_{\pi NN}}{2M}\ , \tag{25}$$

where $\overline{M}$ is the average of the Λ and nucleon masses. The correlated PV amplitude, involving a weak scalar and a strong pseudoscalar (or pseudovector) pion vertex, can be easily derived following the same lines that led to Eq. (12). We finally obtain

$$\tilde{M}_{\rm PC}(\mathbf{k}) = \frac{G_F\mu^2 B}{2\overline{M}}\frac{g_{\pi NN}}{2M}\int d^3r e^{i\mathbf{k}\cdot\mathbf{r}} f(r)\int \frac{d^3q}{(2\pi)^3}\frac{e^{-i\mathbf{q}\cdot\mathbf{r}}}{\mathbf{q}^2+\mu^2}\boldsymbol{\sigma}_1\mathbf{q}\,\boldsymbol{\sigma}_2\mathbf{q},$$

$$\tilde{M}_{\rm PV}(\mathbf{k}) = -G_F\mu^2 A\frac{g_{\pi NN}}{2M}\int d^3r e^{i\mathbf{k}\cdot\mathbf{r}} f(r)\int \frac{d^3q}{(2\pi)^3}\frac{e^{-i\mathbf{q}\cdot\mathbf{r}}}{\mathbf{q}^2+\mu^2}\boldsymbol{\sigma}_2\mathbf{q}\ . \tag{26}$$

In order to clarify further the differences between this approach, consistent with the microscopic model for correlations, and that of Ref. [7], we note that following the steps that led to Eq. (11) we would obtain

$$\tilde{M}_{\rm PC}(\mathbf{k}) = \frac{G_F\mu^2 B}{2\overline{M}}\frac{g_{\pi NN}}{2M}\boldsymbol{\sigma}_1\mathbf{k}\,\boldsymbol{\sigma}_2\mathbf{k}\int d^3r e^{i\mathbf{k}\cdot\mathbf{r}} f(r)\frac{e^{-\mu r}}{4\pi r},$$

$$\tilde{M}_{\rm PV}(\mathbf{k}) = -G_F\mu^2 A\frac{g_{\pi NN}}{2M}\boldsymbol{\sigma}_2\mathbf{k}\int d^3r e^{i\mathbf{k}\cdot\mathbf{r}} f(r)\frac{e^{-\mu r}}{4\pi r}\ . \tag{27}$$

Equations (26) and (27) are the elementary $\Lambda N \to NN$ correlated transition amplitudes in momentum space for the two procedures of including correlations.

The nonmesonic decay rate is given as [7]

$$\Gamma = \int\frac{d^3P}{(2\pi)^3}\int\frac{d^3k}{(2\pi)^3}\overline{\sum}(2\pi)\delta(M_H - E_R - E_1 - E_2)\ |\ \langle\psi_R;\mathbf{P}\mathbf{k}\ S\,M_S\ T\,M_T|\,\hat{O}_{\Lambda N\to NN}\,|_\Lambda A\rangle\ |^2\,, \tag{28}$$

where M_H, E_R, E_1, and E_2 are the mass of the hypernucleus, the energy of the residual $(A-2)$-particle system, and the total asymptotic energies of the emitted nucleons, respectively. A transformation to the center of mass and relative momenta of the two outgoing nucleons is implied in Eq. (28). The sum $\overline{\sum}$ indicates an average over the initial hypernucleus spin projections M_J and sum over all quantum numbers of the residual $(A-2)$-particle system, as well as the spin and isospin projections of the exiting nucleons. We neglect final state distortions as we are studying an inclusive process where the nucleons are still detected even if they undergo inelastic collisions. Therefore, the antisymmetric state of the two final nucleons moving with center-of-mass momentum $\mathbf{P}$ and relative momentum $\mathbf{k}$ can be written as

$$\langle\mathbf{R}\,\mathbf{r}|\,\mathbf{P}\,\mathbf{k}\ S\,M_S\ T\,M_T\rangle = \frac{1}{\sqrt{2}}e^{i\mathbf{P}\cdot\mathbf{R}}\left[e^{i\mathbf{k}\cdot\mathbf{r}} - (-1)^{S+T}e^{-i\mathbf{k}\cdot\mathbf{r}}\right]\chi^S_{M_S}\chi^T_{M_T}$$

$$= \frac{1}{\sqrt{2}}e^{i\mathbf{P}\cdot\mathbf{R}}\sum_{L\,M_L} 4\pi i^L\left[1-(-1)^{L+S+T}\right] j_L(kr)Y^*_{L\,M_L}(\hat{\mathbf{k}})Y_{L\,M_L}(\hat{\mathbf{r}})\chi^S_{M_S}\chi^T_{M_T}\ , \tag{29}$$

where a partial wave expansion for the relative motion plane wave has been made. Following Ref. [7], a weak coupling scheme, in which the Λ in an orbit $\alpha_\Lambda = \{n_\Lambda, l_\Lambda, j_\Lambda, m_\Lambda\}$ couples to the ground state of the nuclear $(A-1)$ core, is assumed for the hypernuclear wave function. Employing the technique of coefficients of fractional parentage, the core wave function is further decomposed into a set of states where the nucleon in an orbit $\alpha_N = \{n_N, l_N, j_N, m_N\}$ is coupled to a residual $(A-2)$-particle state. In the present work, the single particle Λ and N orbits are taken as solutions of a harmonic oscillator potential with appropriate parameters b_Λ and b_N. Assuming an average size parameter $b = (b_\Lambda + b_N)/2$, using Moshinski brackets [11], and working in the LS representation, the product of the two harmonic-oscillator single-particle states can be transformed to a combination of relative and center-of-mass wave functions. With all these ingredients, the many-body transition amplitude of Eq. (28) can be written in terms of two-body amplitudes of the type

$$t_{\Lambda N\to NN} = \int d^3R \int d^3r e^{-i\mathbf{P}\cdot\mathbf{R}} \psi^*_{\mathbf{k}}(\mathbf{r}) \chi^{\dagger S}_{M_S} \tilde{V}(\mathbf{r}) \Phi^{\rm rel}_{n_r l_r}(\mathbf{r};\sqrt{2}b) \Phi^{\rm c.m.}_{n_R l_R}(\mathbf{R};b/\sqrt{2}) \chi^{S_0}_{M_{S_0}}$$
$$= (-i)^{l_R} \Phi^{\rm c.m.}_{n_R l_R}(\mathbf{K};b/\sqrt{2}) \int d^3r \psi^*_{\mathbf{k}}(\mathbf{r}) \chi^{\dagger S}_{M_S} \tilde{V}(\mathbf{r}) \Phi^{\rm rel}_{n_r l_r}(\mathbf{r};\sqrt{2}b) \chi^{S_0}_{M_{S_0}}$$
$$= (-i)^{l_R} \Phi^{\rm c.m.}_{n_R l_R}(\mathbf{K};b/\sqrt{2})\, t_{\rm rel} \ , \tag{30}$$

where isospin indices have been omitted for simplicity. The functions $\Phi_{nl}(\mathbf{a};b)$ are solutions of the three-dimensional harmonic oscillator and $\tilde{V}(\mathbf{r})$ is the correlated potential obtained as a Fourier transform of the nonrelativistic reduction of the correlated Feynman amplitude [Eqs. (26) or (27)].

Writing

$$\tilde{V}(\mathbf{r}) = \tilde{V}_C(r)\boldsymbol{\sigma}_1\boldsymbol{\sigma}_2 + \tilde{V}_T(r) S_{12}(\hat{\mathbf{r}}) + \tilde{V}_{\rm PV}(r)\boldsymbol{\sigma}_2\hat{\mathbf{r}} \ , \tag{31}$$

and assuming the lambda and the nucleon in their lowest $l = 0$ single-particle states, we obtain

$$t^C_{\rm rel} = \delta_{S\,S_0}\delta_{M_S\,M_{S_0}} \sqrt{4\pi}\, 2 \left[S(S+1) - \frac{3}{2}\right] \int dr r^2 j_0(kr) \tilde{V}_C(r) \Phi_{100}(r;\sqrt{2}b), \tag{32}$$

$$t^T_{\rm rel} = -\delta_{M_S\,M_{S_0}} \sqrt{4\pi}\sqrt{6} \sqrt{\frac{2S+1}{2S_0+1}} \frac{\langle S||\,[\sigma_1\otimes\sigma_2]^{J=2}\,||S_0\rangle}{\sqrt{2S+1}} \langle 20\ SM_S|\,S_0M_{S_0}\rangle$$
$$\times \int dr r^2 j_2(kr) \tilde{V}_T(r) \Phi_{100}(r;\sqrt{2}b), \tag{33}$$

$$t^{\rm PV}_{\rm rel} = -\delta_{M_S\,M_{S_0}} \sqrt{4\pi} \sqrt{\frac{2S+1}{2S_0+1}} \frac{\langle S||\,\sigma_2\,||S_0\rangle}{\sqrt{2S+1}} \langle 10\ SM_S|\,S_0M_{S_0}\rangle$$
$$\times \int dr r^2 j_1(kr) \tilde{V}_{\rm PV}(r) \Phi_{100}(r;\sqrt{2}b) \ . \tag{34}$$

For nucleons in a p-shell orbit slightly more complicated expressions are obtained [12].

IV. WEAK $\Lambda N \to NN$ CORRELATED POTENTIAL

In this section we derive the correlated potential in r space by Fourier transforming the nonrelativistic reduction of the corresponding Feynman amplitude. We start considering the procedure of the nonrelativistic calculations giving rise to Eq. (26) which is directly the Fourier transform of the $\mathbf{r}$-dependent potential

$$\tilde{V}^{\rm PC} = V^{\rm PC}(\mathbf{r}) f(r),$$
$$\tilde{V}^{\rm PV} = V^{\rm PV}(\mathbf{r}) f(r) \ , \tag{35}$$

with

$$V^{\rm PC}(\mathbf{r}) = \frac{G_F\mu^2 B}{2\overline{M}} \frac{g_{\pi NN}}{2M} \int \frac{d^3q}{(2\pi)^3} \frac{e^{-i\mathbf{q}\cdot\mathbf{r}}}{\mathbf{q}^2+\mu^2} \boldsymbol{\sigma}_1\mathbf{q}\,\boldsymbol{\sigma}_2\mathbf{q}$$
$$= -\frac{G_F\mu^2 B}{2\overline{M}} \frac{g_{\pi NN}}{2M} \sigma_{1i}\sigma_{2j}\nabla_i\nabla_j \int \frac{d^3q}{(2\pi)^3} \frac{e^{-i\mathbf{q}\cdot\mathbf{r}}}{\mathbf{q}^2+\mu^2}$$
$$= -\frac{G_F\mu^2 B}{2\overline{M}} \frac{g_{\pi NN}}{2M} \sigma_{1i}\sigma_{2j}\nabla_i\nabla_j \frac{e^{-\mu r}}{4\pi r},$$

$$V^{\rm PV}(\mathbf{r}) = -G_F\mu^2 A \frac{g_{\pi NN}}{2M} \int \frac{d^3q}{(2\pi)^3} \frac{e^{-i\mathbf{q}\cdot\mathbf{r}}}{\mathbf{q}^2+\mu^2} \boldsymbol{\sigma}_2\mathbf{q}$$
$$= -iG_F\mu^2 A \frac{g_{\pi NN}}{2M} \sigma_{2i}\nabla_i \frac{e^{-\mu r}}{4\pi r} \ . \tag{36}$$

Using the identities

$$\nabla_i h(r) = \frac{x_i}{r}\frac{dh(r)}{dr},$$
$$\nabla_i\nabla_j h(r) = \delta_{ij}\nabla^2 h(r)$$
$$+(\hat{x}_i\hat{x}_j - \tfrac{1}{3}\delta_{ij}) \left[\frac{d^2h(r)}{dr^2} - \frac{1}{r}\frac{dh(r)}{dr}\right] \ , \tag{37}$$

Eqs. (35) and (36) can be written as

$$\tilde{V}^C = -\frac{G_F\mu^2 B}{2\overline{M}} \frac{g_{\pi NN}}{2M} \frac{1}{3} \left(\mu^2 \frac{e^{-\mu r}}{4\pi r} - \delta(\mathbf{r})\right) f(r)\boldsymbol{\sigma}_1\boldsymbol{\sigma}_2,$$
$$\tilde{V}^T = -\frac{G_F\mu^2 B}{2\overline{M}} \frac{g_{\pi NN}}{2M} \frac{1}{3} \mu^2 \frac{e^{-\mu r}}{4\pi r} \left(1 + \frac{3}{\mu r} + \frac{3}{(\mu r)^2}\right)$$
$$\times f(r) S_{12}(\hat{\mathbf{r}}),$$
$$\tilde{V}^{\rm PV} = iG_F\mu^2 A \frac{g_{\pi NN}}{2M} \mu \frac{e^{-\mu r}}{4\pi r} \left(1 + \frac{1}{\mu r}\right) f(r) \boldsymbol{\sigma}_2\hat{\mathbf{r}} \ . \tag{38}$$

In order to illustrate more explicitly the differences with the results obtained in Ref. [7] we also derive the r-space potential corresponding to Eq. (27). We must then calculate the integrals

$$\int \frac{d^3k}{(2\pi)^3} e^{-i\mathbf{k}\cdot\mathbf{r}} \boldsymbol{\sigma}_1\mathbf{k}\,\boldsymbol{\sigma}_2\mathbf{k} \int d^3r' e^{i\mathbf{k}\cdot\mathbf{r}'} f(r') \frac{e^{-\mu r'}}{4\pi r'}, \tag{39}$$

$$\int \frac{d^3k}{(2\pi)^3} e^{-i\mathbf{k}\cdot\mathbf{r}} \boldsymbol{\sigma}_2\mathbf{k} \int d^3r' e^{i\mathbf{k}\cdot\mathbf{r}'} f(r') \frac{e^{-\mu r'}}{4\pi r'} \ , \tag{40}$$

where we have denoted by $\mathbf{r}'$ the internal coordinate variable. We first perform the momentum integral of Eqs. (39) and (40),

$$\int \frac{d^3k}{(2\pi)^3}\boldsymbol{\sigma}_1\mathbf{k}\,\boldsymbol{\sigma}_2\mathbf{k}\,e^{i\mathbf{k}\cdot(\mathbf{r}'-\mathbf{r})} = -\sigma_{1i}\sigma_{2j}\nabla'_i\nabla'_j\int \frac{d^3k}{(2\pi)^3}e^{i\mathbf{k}\cdot(\mathbf{r}'-\mathbf{r})} = -\sigma_{1i}\sigma_{2j}\nabla'_i\nabla'_j\delta(\mathbf{r}'-\mathbf{r}), \tag{41}$$

$$\int \frac{d^3k}{(2\pi)^3}\boldsymbol{\sigma}_2\mathbf{k}\,e^{i\mathbf{k}\cdot(\mathbf{r}'-\mathbf{r})} = -i\sigma_{2i}\nabla'_i\delta(\mathbf{r}'-\mathbf{r})\ . \tag{42}$$

Next, we perform the integration over $\mathbf{r}'$. Recalling the properties

$$\int d^3r'\,[\nabla'_i\delta(\mathbf{r}'-\mathbf{r})]\,g(\mathbf{r}') = -\nabla_i g(\mathbf{r}), \tag{43}$$

$$\int d^3r'\,[\nabla'_i\nabla'_j\delta(\mathbf{r}'-\mathbf{r})]\,g(\mathbf{r}') = \nabla_i\nabla_j g(\mathbf{r})\ , \tag{44}$$

and using the relations (37), it is straightforward to derive

$$\tilde{V}^C = -\frac{G_F\mu^2 B}{2\overline{M}}\frac{g_{\pi NN}}{2M}\frac{1}{3}\left\{\left(\mu^2\frac{e^{-\mu r}}{4\pi r}-\delta(\mathbf{r})\right)f(r)-\mu^2\frac{e^{-\mu r}}{4\pi r}\left(\frac{2}{\mu}\frac{df}{dr}-\frac{1}{\mu^2}\frac{d^2f}{dr^2}\right)\right\}\boldsymbol{\sigma}_1\boldsymbol{\sigma}_2,$$

$$\tilde{V}^T = -\frac{G_F\mu^2 B}{2\overline{M}}\frac{g_{\pi NN}}{2M}\frac{1}{3}\mu^2\frac{e^{-\mu r}}{4\pi r}\left\{\left(1+\frac{3}{\mu r}+\frac{3}{(\mu r)^2}\right)f(r)-\left(\frac{3}{\mu r}+2\right)\frac{1}{\mu}\frac{df}{dr}+\frac{1}{\mu^2}\frac{d^2f}{dr^2}\right\}S_{12}(\hat{\mathbf{r}}),$$

$$\tilde{V}^{PV} = iG_F\mu^2 A\frac{g_{\pi NN}}{2M}\mu\frac{e^{-\mu r}}{4\pi r}\left\{\left(1+\frac{1}{\mu r}\right)f(r)-\frac{1}{\mu}\frac{df}{dr}\right\}\boldsymbol{\sigma}_2\hat{\mathbf{r}}\ . \tag{45}$$

By comparing Eqs. (38) and (45) we realize that in the approach based on Eq. (27) one obtains new terms in the potential involving first and second derivatives of the correlation function. This explains the different effect of SRC's on the $\Lambda N \to NN$ decay obtained in the approaches of Refs. [2–4] and Ref. [7]. In the former case the correlated potential in coordinate space is simply obtained by multiplying the original one by a correlation function, as seen from Eq. (38). The nonrelativistic equivalent of the procedure of Ref. [7] is a more complicated correlated potential with additional derivative terms.

In our calculation we also include the effect of a πNN form factor. We take a monopole form

$$\frac{\Lambda^2-\mu^2}{\Lambda^2-q^2}\ , \tag{46}$$

at both the weak and the strong πNN vertices. The cutoff mass is taken to be $\Lambda = 1.3$ GeV as needed in the empirical study of the NN interaction. When a form factor is included, the correlated potential of Eq. (38), written as

$$\begin{aligned}
\tilde{V}^C &= -\frac{G_F\mu^2 B}{2\overline{M}}\frac{g_{\pi NN}}{2M}\frac{1}{3}V^C(r;\mu)f(r)\boldsymbol{\sigma}_1\boldsymbol{\sigma}_2,\\
\tilde{V}^T &= -\frac{G_F\mu^2 B}{2\overline{M}}\frac{g_{\pi NN}}{2M}\frac{1}{3}V^T(r;\mu)f(r)S_{12}(\hat{\mathbf{r}}),\\
\tilde{V}^{\rm PV} &= iG_F\mu^2 A\frac{g_{\pi NN}}{2M}V^{\rm PV}(r;\mu)f(r)\boldsymbol{\sigma}_2\hat{\mathbf{r}}\ ,
\end{aligned} \tag{47}$$

gets modified by using the replacements

$$\begin{aligned}
V^C(r;\mu) &\to V^C(r;\mu) - V^C(r;\Lambda)\\
&\quad -\Lambda\frac{\Lambda^2-\mu^2}{2}\frac{e^{-\Lambda r}}{4\pi}\left(1-\frac{2}{\Lambda r}\right),\\
V^T(r;\mu) &\to V^T(r;\mu) - V^T(r;\Lambda)\\
&\quad -\Lambda\frac{\Lambda^2-\mu^2}{2}\frac{e^{-\Lambda r}}{4\pi}\left(1+\frac{1}{\Lambda r}\right),\\
V^{\rm PV}(r;\mu) &\to V^{\rm PV}(r;\mu) - V^{\rm PV}(r;\Lambda) - \frac{\Lambda^2-\mu^2}{2}\frac{e^{-\Lambda r}}{4\pi}\ ,
\end{aligned} \tag{48}$$

where $V^\alpha(r;\Lambda)$ is the same as $V^\alpha(r;\mu)$ but replacing the pion mass μ by the cutoff mass Λ.

V. RESULTS AND DISCUSSION

Once the issue of correlations has been clarified, we can perform a comparative study of the nonmesonic decay width of finite hypernuclei, improving on the results of Ref. [3], where the calculations were done in infinite nuclear matter and the results in finite nuclei were obtained via the local density approximation.

The ${}^{5}_{\Lambda}$He wave function consists of a Λ particle in a $s_{1/2}$ state coupled to the ground state of ^{4}He which has spin parity 0^+. The ^{4}He core is described as four s-shell nucleons moving in a harmonic oscillator potential, with size parameter $b_N = 1.4$ fm, which provides a good description of the ^{4}He charge form factor. The Λ wave function is taken as a solution of a harmonic oscillator

with size parameter $b_\Lambda = 1.85$ fm. This wave function has a similar shape to that obtained with a Woods-Saxon potential adjusted to reproduce the Λ separation energy in ${}^{5}_{\Lambda}$He, $B_\Lambda = -3.12$ MeV. In a similar way, the ${}^{12}_{\Lambda}$C is also represented in terms of harmonic oscillator single-particle wave functions. The parameter $b_N = 1.64$ fm reproduces the ^{12}C charge form factor while $b_\Lambda = 1.87$ fm has been chosen to reproduce the Λ separation energy in ${}^{12}_{\Lambda}$C of $B_\Lambda = -10.7$ MeV. In this case, the model space contains the $s_{1/2}$, $p_{3/2}$, and $p_{1/2}$ orbits, thus allowing configuration mixing to take place within the open p shell.

We will consider different correlation functions which are commonly used in the literature

(i) A Gaussian type

$$f(r) = 1 - e^{-r^2/b^2} , \tag{49}$$

with $b = 0.75$ fm, has been used in Refs. [2,4] in connection with the study of the nonmesonic decay in nuclear matter. This correlation function is represented by the dashed line in Fig. 3.

(ii) A Bessel type

$$f(r) = 1 - j_0(q_c r) , \tag{50}$$

with $q_c = 3.93$ fm^{-1}, was found to provide a good description of the correlation function for nucleon pairs in ^{4}He [13] as calculated with the Reid soft core potential [14]. This correlation function, depicted by the dotted line in Fig. 3, was used in Ref. [3] in the study of the Λ decay in nuclear matter.

(iii) Finally, the parametrization

$$f(r) = \left(1 - e^{-r^2/a^2}\right)^n + br^2 e^{-r^2/c^2} , \tag{51}$$

with $a = 0.5$ fm, $b = 0.25$ fm^{-2}, $c = 1.28$ fm, and $n = 2$, provides a good description of realistic ΛN correlation functions obtained with G-matrix calculations [15,16] using the Nijmegen interaction [17]. This correlation function, depicted by the solid line in Fig. 3, is the one used in the relativistic calculations of Ref. [7] for the nonmesonic decay of finite hypernuclei.

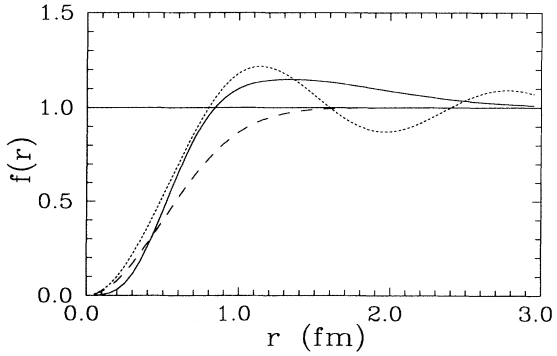

FIG. 3. The ΛN correlation function as a function of the relative distance r. The dashed, dotted, and solid lines correspond to the Gaussian type of Eq. (49), the Bessel type of Eq. (50), and the parametrization of Eq. (51), respectively.

TABLE I. Nonmesonic $\Lambda N \to NN$ decay rate of ${}^{5}_{\Lambda}$He for the relativistic model of Ref. [7] (in units of the free Λ width).

	Free	$f(r)$ [Eq. (51)]
PC= $C + T$	0.637	0.187
PV	0.314	0.137
Total	0.951	0.324

The results of Table I show the effect of including the correlation function of Eq. (51) in the nonmesonic decay rate of ${}^{5}_{\Lambda}$He using the relativistic model of Ref. [7]. Note that a reduction factor of about 3 is obtained with respect to the results of the first column, which do not include short range correlation effects. The reduction on the free rate is twice as large as that obtained with the nonrelativistic models in nuclear matter [2–4]. This was the discrepancy that motivated the present work.

From Sec. II we have learned that these differences must not be attributed to a relativistic effect but rather to the different prescription on how to incorporate the correlations. This can be clearly corroborated by examining the results of Table II, which compares the decay rate of ${}^{5}_{\Lambda}$He, without including form factors, for the two nonrelativistic correlated potentials: (i) the one of Eq. (38), which is the prescription used in Refs. [2–4] and has been shown to be consistent with a microscopic interpretation of short range correlations, and (ii) the one of Eq. (45), which is the nonrelativistic equivalent of the relativistic model used in Ref. [7]. The results are given for the different correlation functions described above. Note that the rate of the fourth column based on the potential of Eq. (45) gives a reduction near to that observed in the relativistic calculations of Ref. [7], shown in Table I, when the same correlation function [Eq. (51)] is used. This comparison corroborates that the origin of the discrepancies in the effect of correlations between the

TABLE II. $\Lambda N \to NN$ decay rate of ${}^{5}_{\Lambda}$He for different correlation functions (in units of the free Λ width).

	Free	$f(r) = 1 - e^{-r^2/b^2}$	
		Eq. (38)	Eq. (45)
C	0.174	9.2×10^{-4}	0.028
T	0.495	0.309	0.077
PV	0.308	0.155	0.059
Total	0.977	0.465	0.164
	Free	$f(r) = 1 - j_0(q_c r)$	
		Eq. (38)	Eq. (45)
C	0.174	2.2×10^{-3}	0.082
T	0.495	0.434	0.233
PV	0.308	0.249	0.156
Total	0.977	0.685	0.471
	Free	$f(r) = \left(1 - e^{-r^2/a^2}\right)^n + br^2 e^{-r^2/c^2}$	
		Eq. (38)	Eq. (45)
C	0.174	1.7×10^{-3}	0.057
T	0.495	0.448	0.159
PV	0.308	0.244	0.117
Total	0.977	0.694	0.333

nonrelativistic approach [2–4] and the relativistic one [7] has nothing to do with relativistic effects and is due to the prescription used to include the correlation function in the transition amplitude. Indeed, the strong reduction obtained with the model of Ref. [7] is reproduced by the nonrelativistic correlated potential of Eq. (45), which is obtained when the pseudoscalar πNN and $\pi N\Lambda$ vertex functions are evaluated between initial and final spinors (as assumed in Ref. [7]) instead of using external and intermediate spinors as the microscopic model for short range correlations requires.

The results of Table II show that, in the standard nonrelativistic calculations of the third column, Eq. (38), the channel more drastically affected by correlations is the central one, the reason being that the correlation functions used here have the property $f(r = 0) = 0$. Since the correlated potential is $V(\mathbf{r})f(r)$, the delta piece of the interaction, which provides most of the contribution for the central channel in the free calculation (second column), is completely supressed. Although the delta contribution is also removed in the prescription based on Eq. (45), the results of the fourth column show that the central strength is considerably larger due to the additional derivative pieces of the correlated potential. The integrand of Eq. (32) is shown in Fig. 4 for the correlation function of Eq. (51). The solid and dotted lines correspond to the correlated central potential of Eqs. (38) and (45) respectively. Because of the change of sign in the derivative of $f(r)$ around 0.5 fm, the correlated transition amplitude based on Eq. (45) shows large positive and negative contributions, which do not cancel each other completely and end up giving an integrated central rate much larger than that obtained from the integral of the solid line in Fig. 4 corresponding to the potential of Eq. (38). On the other hand, it is precisely this oscillatory behavior of the correlated potential given by Eq. (45) that is the reason for the reduced tensor and parity violating rates of the forth column in Table II with respect to those of the third column, obtained with the standard procedure based on Eq. (38). The integrand for the tensor rate is shown in Fig. 5. Here, one finds that the positive and negative parts induced by the derivative terms of the correlated potential of Eq. (45) tend to cancel each other, giving rise to an integrated rate which is considerably smaller than that of the solid line, obtained with the correlated potential of Eq. (38). A similar behavior is obtained for the parity violating rate and, therefore, the total rate based on Eq. (45) ends up being much smaller than that of the appropriate calculation, based on Eq. (38). Depending somewhat on the correlation function used, the rates based on the correlated potential of Eq. (45) are a factor 2–3 smaller than those obtained with Eq. (38). This is an important result since, as already noted before, it explains the discrepancies observed between the relativistic calculations [7] and the nonrelativistic ones [2–4]. Our results, obtained with nonrelativistic reductions of the Feynman amplitude, also corroborate that the differences are inherent to the type of prescription used to account for correlations and cannot be attributed to a relativistic effect.

Results for the nonmesonic decay rate of ${}^{5}_{\Lambda}$He and ${}^{12}_{\Lambda}$C containing also the effect of a form factor are given in Table III, where the correlation function used is the parametrization of Eq. (51). The values $\Gamma_{nm}/\Gamma_{\Lambda} = 0.56$ for ${}^{5}_{\Lambda}$He and $\Gamma_{nm}/\Gamma_{\Lambda} = 0.96$ for ${}^{12}_{\Lambda}$C are consistent with the experimental data [18]. Because of the short range nature of the $\Lambda N \to NN$ transition, it has been argued that the exchange of heavier mesons may also give a relevant contribution to the decay rate. However, recent calculations suggest that, when SRC's and form factors are included, the heavier mesons do not modify the decay rate of ${}^{12}_{\Lambda}$C appreciably [19]. As for ${}^{5}_{\Lambda}$He, we must note that the mean field picture used in the present work is a quite crude model and calculations based on a more microscopic picture of the hypernuclear wave function are needed. We have used a shell model wave function for the Λ while it is known [20] that the short range ΛN repulsion pushes the Λ wave function to the surface of the nucleus. Then the overlap with the nucleons becomes smaller and produces a reduced decay rate. According

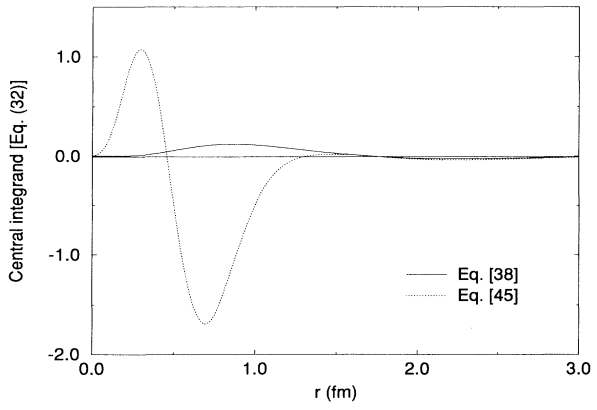

FIG. 4. Integrand of the central transition amplitude [see Eq. (32)], in arbitrary units, as a function of the relative distance r. The solid and dotted lines correspond to the correlated potential of Eqs. (38) and (45), respectively, using the correlation function of Eq. (51).

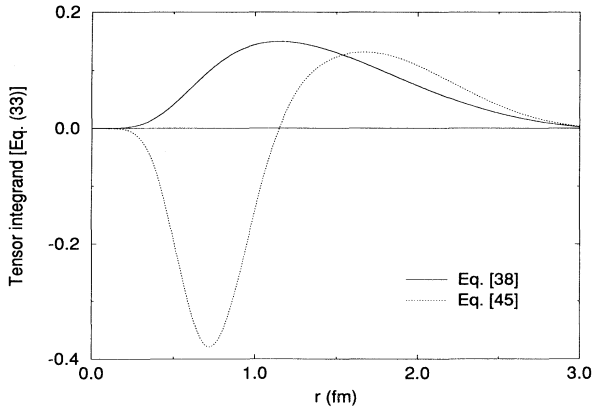

FIG. 5. The same as Fig. 4 for the tensor transition amplitude [see Eq. (33)].

TABLE III. $\Lambda N \to NN$ decay rate of ${}^{5}_{\Lambda}$He and ${}^{12}_{\Lambda}$C including SRC's and form factors (FF) (in units of the free Λ width).

	${}^{5}_{\Lambda}$He			${}^{12}_{\Lambda}$C		
	Free	SRC's	SRC's + FF	Free	SRC's	SRC's + FF
C	0.174	0.002	0.008	0.285	0.003	0.013
T	0.495	0.448	0.363	0.843	0.764	0.621
PV	0.308	0.244	0.189	0.513	0.419	0.330
Total	0.977	0.694	0.560	1.641	1.186	0.964
Expt [18]		0.41 ± 0.14			1.14 ± 0.20	

to Ref. [21], this reduction is of the order of 40% and this would produce a nonmesonic rate in ${}^{5}_{\Lambda}$He of the order of $0.34\Gamma_{\Lambda}$, which is more consistent with experiment.

The fact that the one-pion-exchange mechanism provides nonmesonic $\Lambda N \to NN$ rates close to experiment should not make us forget that it fails badly to provide the ratio of neutron to proton induced Λ decay [6]. It is, however, shown in Ref. [19] that the addition of other meson exchanges can alter substantially this ratio while leaving the nonmesonic rate practically unchanged.

VI. CONCLUSIONS

The main aim of this paper has been to find the reasons for the discrepancies found in the literature on the effect of short range correlations in the nonmesonic decay width of Λ hypernuclei. The rates obtained in the relativistic model developed in Ref. [7] were much smaller than the nonrelativistic calculations of Refs. [2–4], suggesting that relativistic effects might be very important in the nonmesonic Λ decay.

We have shown that the discrepancies are not due to relativistic effects but to the way the short range correlations are implemented. First, we showed that the prescription to include correlations used in Ref. [7] leads to different results if one uses pseudoscalar or pseudovector πNN couplings, the latter one with the derivative acting on the pion field. This already shows a pathology in the approach used to include correlations in Ref. [7], since in the present problem one only needs matrix elements between positive energy components, where, in the usual nonrelativistic approximation, these two couplings are equivalent.

In order to understand the origin of this pathology we constructed a schematic microscopic model for the short range effects which provided us with the right way to include the correlations by means of a correlation function. This allowed us to show that the prescription followed in Ref. [7] is incorrect because it factorizes the matrix elements of the vertices as a function of the external variables, while in the appropriate method they appear as a function of the momentum in the loop integral involved in the correlated amplitudes. This correct prescription is equivalent to multiplying the potential, written fully in coordinate space, by the correlation function, which is the procedure followed in Refs. [2–4]. However, the nonrelativistic potential obtained with the procedure of Ref. [7] gives rise to additional terms involving derivatives of the correlation function.

A quantitative comparison of the ${}^{5}_{\Lambda}$He nonmesonic decay rate obtained by both procedures has shown that the correct prescription gives moderate reductions of about 30% instead of reductions of about a factor of 3 found by the incorrect one. This study has also corroborated that the differences on the rates observed between the relativistic model of Ref. [7] and the nonrelativistic approach of Refs. [2–4] cannot be attributed to relativistic effects.

By taking the correct correlated potential, a realistic correlation function, and form factors at the vertices, we have obtained results for the nonmesonic decay width of ${}^{5}_{\Lambda}$He and ${}^{12}_{\Lambda}$C, using also realistic wave functions for the finite nucleus instead of the infinite nuclear matter approach of Refs. [2–4]. We obtain a very close agreement with the experimental data, especially in the case of ${}^{12}_{\Lambda}$C for which a mean field description of the wave function is a rather realistic picture. For ${}^{5}_{\Lambda}$He, the additional consideration of dynamical effects tied to the short range ΛN repulsion, which pushes the Λ wave function more to the surface of the nucleus, also brings the results in good agreement with experiment.

ACKNOWLEDGMENTS

We would like to thank C. Bennhold, E.D. Cooper, and B.K. Jennings for fruitful discussions and valuable comments. This work has been partially supported by CICYT Contract No. AEN 93-1205 and DGICYT Contract No. PB92-0761 (Spain). A.P. acknowledges support from the Ministerio de Educación y Ciencia (Spain).

[1] J.B. Adams, Phys. Rev. **156**, 1611 (1967).
[2] B.H.J. McKellar and B.F. Gibson, Phys. Rev. C **30**, 322 (1984).
[3] E. Oset and L.L Salcedo, Nucl. Phys. **A433**, 704 (1985).
[4] J.F. Dubach, Nucl. Phys. **A450**, 71c (1986).
[5] D.P. Heddle and L.S. Kisslinger, Phys. Rev. C **33**, 608 (1986).
[6] J. Cohen, in *Progress in Particle and Nuclear Physics*, edited by A. Faessler (Pergamon Press, New York, 1990), Vol. 25, p. 139.

[7] A. Ramos, C. Bennhold, E. van Meijgaard, and B.K. Jennings, Phys. Lett. B **264**, 233 (1991); A. Ramos, E. van Meijgaard, C. Bennhold, and B.K. Jennings, Nucl. Phys. **A544**, 703 (1992).
[8] W.M. Alberico, A. De Pace, M. Ericson, and A. Molinari, Phys. Lett. B **256**, 134 (1991).
[9] A. Ramos, E. Oset, and L.L. Salcedo, Phys. Rev. C **50**, 2314 (1994).
[10] G.E. Brown and A.D. Jackson, *The Nucleon-Nucleon Interaction* (North-Holland, Amsterdam, 1976), p. 75.
[11] M. Moshinski, Nucl. Phys. **13**, 104 (1959).
[12] A. Parreño, A. Ramos, and C. Bennhold (work in progress).
[13] W. Weise, Nucl. Phys. **A278**, 402 (1977).
[14] R.V. Reid, Ann. Phys. (N.Y.) **50**, 411 (1968).
[15] H. Bandō, Prog. Theor. Phys. Suppl. **81**, 181 (1985).
[16] D. Halderson, Phys. Rev. C **48**, 581 (1993).
[17] M.N. Nagels, T.A. Rijken, and J.J. de Swart, Phys. Rev. D **15**, 2547 (1977); P.M.M. Maessen, Th.A. Rijken, and J.J. de Swart, Phys. Rev. C. **40**, 2226 (1989).
[18] J.J. Szymanski *et al.*, Phys. Rev. C **43**, 849 (1991).
[19] A. Ramos and C. Bennhold, Nucl. Phys. **A585**, 375c (1995).
[20] U. Straub, J. Nieves, A. Faessler, and E. Oset, Nucl. Phys. **A566**, 531 (1993).
[21] E. Oset, L.L. Salcedo, and Q.N. Usmani, Nucl. Phys. **A450**, 67c (1986).